Bulletin of the Seismological Society of America, Vol. 87, No. 2, pp. 294–309, April 1997

Transient Triggering of Near and Distant Earthquakes

by Joan Gomberg, Michael L. Blanpied, and N. M. Beeler

Abstract We demonstrate qualitatively that frictional instability theory provides a context for understanding how earthquakes may be triggered by transient loads associated with seismic waves from near and distance earthquakes. We assume that earthquake triggering is a stick-slip process and test two hypotheses about the effect of transients on the timing of instabilities using a simple spring-slider model and a rate- and state-dependent friction constitutive law. A critical triggering threshold is implicit in such a model formulation.

Our first hypothesis is that transient loads lead to clock advances; i.e., transients hasten the time of earthquakes that would have happened eventually due to constant background loading alone. Modeling results demonstrate that transient loads do lead to clock advances and that the triggered instabilities may occur after the transient has ceased (i.e., triggering may be delayed). These simple "clock-advance" models predict complex relationships between the triggering delay, the clock advance, and the transient characteristics. The triggering delay and the degree of clock advance both depend nonlinearly on when in the earthquake cycle the transient load is applied. This implies that the stress required to bring about failure does not depend linearly on loading time, even when the fault is loaded at a constant rate. The timing of instability also depends nonlinearly on the transient loading rate, faster rates more rapidly hastening instability. This implies that higher-frequency and/or longer-duration seismic waves should increase the amount of clock advance. These modeling results and simple calculations suggest that near (tens of kilometers) small/moderate earthquakes and remote (thousands of kilometers) earthquakes with magnitudes 2 to 3 units larger may be equally effective at triggering seismicity.

Our second hypothesis is that some triggered seismicity represents earthquakes that would not have happened without the transient load (i.e., accumulated strain energy would have been relieved via other mechanisms). We test this using two "new-seismicity" models that (1) are inherently unstable but slide at steady-state conditions under the background load and (2) are conditionally stable such that instability occurs only for sufficiently large perturbations. For the new-seismicity models, very small-amplitude transients trigger instability relative to the clock-advance models. The unstable steady-state models predict that the triggering delay depends inversely and nonlinearly on the transient amplitude (as in the clock-advance models). We were unable to generate delayed triggering with conditionally stable models. For both new-seismicity models, the potential for triggering is independent of when the transient load is applied or, equivalently, of the prestress (unlike in the clock-advance models). In these models, a critical triggering threshold appears to be inversely proportional to frequency. Further advancement of our understanding will require more sophisticated, quantitative models and observations that distinguish between our qualitative, yet distinctly different, model predictions.

Introduction

We present results of heuristic models of earthquake triggering, based on the behavior of a simple spring-slider system as a model of fault slip governed by rate-state constitutive laws (Dieterich, 1979, 1986; Ruina, 1983). Our application differs from earlier spring-slider models (Dieterich, 1979, 1981, 1986, 1994; Rice and Gu, 1983; Gu *et al.*, 1984;

Carlson and Langer, 1989; Carlson *et al.,* 1991; Gu and Wong, 1991; Dieterich and Kilgore, 1996) in that we focus on "dynamic" triggering, seismicity (i.e., slip) initiated by stress or strain changes associated with passing seismic waves. Dynamic triggering has been proposed to explain the distant seismicity triggered by the M 7.3 Landers, California, earthquake (Hill *et al.,* 1993, 1995; Anderson *et al.,* 1994; Gomberg and Bodin, 1994; Gomberg, 1996) and remotely triggered seismicity at The Geysers, California (Gomberg and Davis, 1996). We demonstrate that dynamic triggering can plausibly explain remote seismicity, even that which occurs with considerable delay between the passage of the triggering transient and the onset of triggered activity. Note that herein the term "triggered" differs from some others in that the triggered event may occur at any time; e.g., Hill *et al.* (1993) required that the timing of triggered activity meet certain statistical criteria in order to identify it in real earthquake catalogs. We do not impose such restrictions because our objective is not to solve the observational problem of how to identify triggered seismicity. Our goal is to test the feasibility of dynamic triggering by beginning with simple hypotheses and models—we do not attempt to model the complex mechanics of faulting in the real Earth.

Dynamic triggering also may be considered as a possible mechanism for generation of aftershocks and multiple-earthquake sequences. Heretofore, most studies have hypothesized that static stress changes that move a fault closer to satisfying a Coulomb frictional failure criterion (often called Coulomb failure stress changes) promote aftershocks and earthquake sequences (Das and Scholz, 1981; Stein and Lisowski, 1983; Dieterich, 1986; Reasenberg and Simpson, 1992; Harris and Simpson, 1992; Jaume and Sykes, 1992; Stein *et al.,* 1992; Du and Aydin, 1993; King *et al.,* 1994; Dodge *et al.,* 1995; Harris *et al.,* 1995). Some of these studies conclude that static Coulomb failure stress changes alone cannot initiate rupture (Harris and Simpson, 1992), and others conclude that the relevance of such changes remains elusive (Du and Aydin, 1993; Dodge *et al.,* 1995). Considerable attention has been paid to the potential for static stress changes to advance the time of fault failure (referred to as clock advances) (Harris and Simpson, 1992; Stein *et al.,* 1992; Jaume and Sykes, 1992; King *et al.,* 1994), because such advances may alter estimates of earthquake probabilities. Our modeling experiments suggest that dynamic stress changes also cause clock advances. Furthermore, unlike most previous triggering studies, we consider the possibility that (static or dynamic) triggering does not simply represent an advance of the time of failure but rather that it induces earthquakes that would not have occurred under a constant background load alone (see also Hill *et al.,* 1995; Gomberg and Davis, 1996). These considerations add complicating dimensions to seismic hazard evaluation.

The implications of dynamic triggering are profound, albeit extremely difficult to test observationally. That is, the timing and/or potential for future earthquakes depends not only on the localized static stress changes associated with past earthquakes but also by the more far-reaching, transient seismic waves (and any aseismic transients) they generate. We cite a few examples of apparent far-reaching connections between earthquakes to demonstrate the plausibility of triggering by transient seismic waves emanating from a distant source, acknowledging that other causative processes also may be partly or completely responsible. [For summaries of other possible processes, see Rice and Gu (1983) and Hill *et al.* (1993, 1995).] The most unambiguous example of dynamically triggered seismicity is that which followed the Landers earthquake. Obvious increases in seismicity rates occurred within seconds to days after the Landers earthquake, as far as 1250 km from the Landers epicenter (Hill *et al.,* 1993). Other cases of smaller increases in seismicity rates triggered by large remote (distances greater than several source dimensions) earthquakes have been documented in Japan (Kanamori, 1972), Costa Rica (Protti *et al.,* 1995), and Mexico (Singh *et al.,* 1996). A common perception is that triggered seismicity correlates with young volcanism and geothermal activity. In the one study that examined this rigorously, Anderson *et al.* (1994) concluded that this correlation probably does not exist. They showed that only a small number of Landers-triggered earthquakes correlated with regions of young volcanism and that while an extensive correlation with high heat flow cannot be ruled out, in numerous geothermal areas, seismicity was not triggered. Anderson *et al.* (1994) suggested that triggered activity may correlate with regions of high seismicity, thus leading to an apparent correlation with recent volcanism and geothermal activity that tend to have high seismicity rates. However, they also concluded that none of these conditions alone, high seismicity, recent volcanism, or geothermal activity, were sufficient conditions for extensive triggering.

Earthquake prediction schemes that monitor seismicity changes within areas an order of magnitude larger than the potential mainshock source dimension explicitly assume long-range interactions (Keilis-Borok and Kossobokov, 1990; Kossobokov and Carlson, 1995); theoretical modeling (Pepke *et al.,* 1994) and empirical data (Kagan and Jackson, 1991) validate such assumptions. Rice and Gu (1983) cite examples of apparently related Chinese earthquakes, separated by 480 to >1100 km. Press and Allen (1995) use a pattern recognition algorithm with regional seismicity records and conclude that seismicity in the Great Basin and Gulf of California may modulate seismically accommodated deformation in southern California.

Model Parameterization

We explore the characteristics of instability behavior for a simple massless spring-slider system. Numerous previous studies have used the spring-slider block model of a one-dimensional fault because it is the simplest model that incorporates both a "fault" (a frictional sliding surface) and elastic surroundings through which the fault is loaded (albeit approximately). The stored elastic stress in the country rock,

or equivalently in the spring, is relaxed when the shear traction on the fault drops to zero. In such a model (Fig. 1), the shear stress in two elastic blocks, each driven at a distance L from a fault with a fault-parallel relative displacement D, equals DG/L, where G is the rigidity of the block. The stress relaxed on the fault equals Gd/L for a simple dislocation with displacement d on fault length L. The fault length equals the loading distance because for a dislocation on a fault with length L, the stress is relieved in a volume with radius $\sim L$ (Bodin and Bilham, 1994). G/L is the fault or block stiffness (equivalent to the spring stiffness in the slider model) (Dieterich, 1978).

The essence of our model is a modified rate-state constitutive frictional law in which the coefficient of friction at the base of the slider is

$$\mu(t) = \mu_0 + a \ln[V(t)/V_0] + b \ln[\xi(t)V_0/d_c] \quad (1)$$

(Dieterich, 1986). The state variable, ξ, is a function of time, t, and slider velocity, V. The rate of change of ξ is governed by the evolution law

$$d\xi(t)dt = 1 - \xi(t)\, V(t)/d_c \quad (2)$$

(Ruina, 1983). Here d_c represent a critical slip distance, and μ_0 and V_0 are a reference frictional coefficient and velocity, respectively. a and b are dimensionless parameters. The potential for instability requires that $b > a$ (Rice and Ruina, 1983). A number of physical interpretations may be ascribed to ξ and d_c. ξ may be thought to represent the contact area (Scholz, 1990), the time scale over which contact surfaces evolve (Dieterich, 1979, 1981), the width of the actively deforming shear zone (Marone and Kilgore, 1993), or a function of the porosity of fault-zone material (Sleep, 1995; Segall and Rice, 1995). d_c may be thought of as the displacement on the fault surface required to change the population of contact points (Dieterich, 1979, 1981). The behaviors described by equations (1) and (2) have been tested extensively in the laboratory, and values for d_c, μ_0, a, and b have been measured for a variety of fault materials (e.g., Dieterich, 1978, 1981; Tullis and Weeks, 1986; Marone *et al.*, 1990; Blanpied *et al.*, 1991; Marone and Kilgore, 1993). Model and laboratory experiments demonstrate that faults governed by equations (1) and (2) may display a rich variety of sliding behaviors, analogous to natural faults.

The system is loaded at a constant background rate, V_b, and by a transient load. The background load may be considered analogous to strain accumulation due to plate motion, and the transient displacement, $x(t)_T$, to strains associated with the passage of seismic waves. For simplicity, we assume a single load point for both background and transient loading. Mathematically, we write the load point displacement due to the background and transient loads as

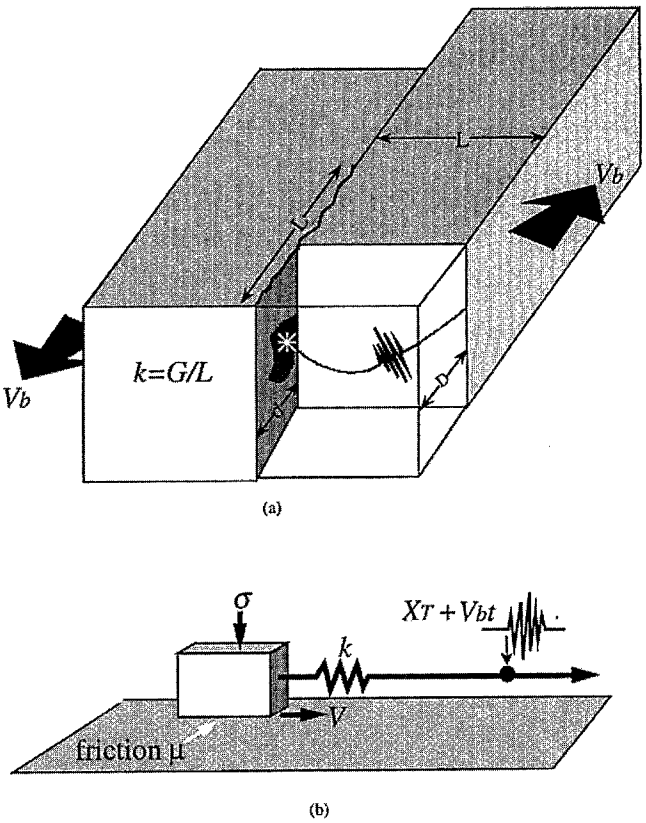

Figure 1. (a) Drawing of a fault model (modified from Dieterich *et al.*, 1978; Sleep and Blanpied, 1992, 1994). Two blocks of elastic material, separated by a vertical fault, undergo relative displacement D, being driven from a distance L with a fault-parallel constant velocity V_b. L also corresponds to the length of fault that slips by amount d. The fault and material stiffness equals G/L in which G is the rigidity of the blocks. The fault patch (darker area on fault surface) may also be loaded by a transient displacement (oscillatory signal). (b) Drawing of the spring-slider model that is analogous to the fault model in (a). A constant normal stress, σ, is applied to a massless block that sits on a frictional surface, connected to a spring with spring constant k. The load point is displaced a distance $X_T(t) + V_b t$ (t is time, V_b represents a constant velocity background load, and $X_T(t)$ is a transient load) causing the slider to move with velocity V. The motion of the slider and friction, μ, is governed by a rate-state-dependent constitutive law (equation 1).

$$x_{lp}(t) = V_b t + x(t)_T \quad (3a)$$

so that the load point velocity is

$$dx_{lp}(t)/dt = V_b + dx(t)_T/dt. \quad (3b)$$

The velocity of the slider is V. Strain energy accumulates because of the difference in displacement of the load point and slider. We study the system's response for various transient load characteristics by monitoring the slider stability with time, as inferred from the evolution of μ, V, and ξ. The

evolution of μ is governed by the change in shear stress, τ, assuming a constant normal stress, σ, analogous to lithostatic stress in the real Earth and fault-parallel loading, and neglecting inertial forces (i.e., a massless slider). [A more general model could include inertia and changing normal stress; e.g. see Rice and Tse (1986), Linker and Dieterich (1992), and Sleep (1995).] The change in τ is proportional to the spring constant $K = k\sigma$ in which k is the system stiffness. Mathematically, this may be written as

$$d\tau/dt = \sigma d\mu/dt = \sigma k(dx_{lp}/dt - V). \quad (4)$$

Thus, the rate of change of μ at any time may be calculated according to

$$d\mu(t)/dt = k[dx_{lp}(t)/dt - V(t)] \quad (5)$$

(Dieterich, 1981).

At each time step, the derivatives of μ, x_{lp}, and ξ are calculated according to equations (1), (2), (3b), and (5), respectively; μ, x_{lp}, and ξ at subsequent time steps are calculated using a Runga–Kutta algorithm (Press *et al.*, 1986). At each time step, the slider velocity is calculated from equation (1):

$$\ln[V(t)/V_0] = \{\mu(t) - \mu_0 - b \ln[\xi(t)V_0/d_c]\}/a. \quad (6)$$

At the time of mechanical system instability, the calculations become numerically unstable and are stopped.

Physical instabilities arise when the fault strength decreases with slip at a rate greater than does the resisting force associated with the elastic stiffness of the surrounding material. Equations (1) and (2) describe the changing strength of the fault or slider, and equation (4) describes the interaction with the surrounding material. A requirement for instability is that slip exceed d_c; this is consistent with a critical threshold for earthquake triggering (Gomberg and Davis, 1996; Roy and Marone, 1996). In addition, instability is guaranteed if the system stiffness is less than a critical value, k_c, or

$$k < k_c, \quad k_c = (b - a)/d_c, \quad (7)$$

except when the system is exactly at steady state (Rice and Ruina, 1983). (Note that for $a > b$, $k_c < 0$, and the system is stable for any value of k.) Steady-state conditions imply that $d\xi/dt = 0$. When loaded at a constant rate V_b, the steady-state velocity, V_{ss}, must equal V_b, and the steady-state model variables are

$$\begin{aligned} V(t) &= V_{ss} = V_b, \\ \xi(t) &= d_c/V_{ss}, \\ \mu(t) &= \mu_0 + (a - b) \ln(V_{ss}/V_0). \end{aligned} \quad (8)$$

We test two end-member hypotheses. In the clock-advance hypothesis, the transient loads simply advance the time of instabilities that would have happened due to the background load. In this case, parameters are selected so that the system is unstable ($k < k_c$) and is not initially at steady state. In the new-seismicity hypothesis, the transient loads cause instabilities to occur that would not have otherwise. In this case, either the system is conditionally stable ($k > k_c$) and the transient "pushes" it over the stability boundary or it is inherently unstable ($k < k_c$) but begins with steady-state conditions prevailing (equation 8).

Equation (1) constrains the motion of the slider so that V cannot be negative and thus the slider cannot go backward (positive V and V_b implying motion in the same direction). This does not seem restrictive for constant-rate background loading, but as will be shown, it is a key constraint on the slider response to an oscillatory transient load. Although the load point may move forward and backward, the slider responds only by changing the rate at which it moves forward. Relating this to loading of faults, it implies that a transient load only can affect the rate at which strain accumulates on the fault and cannot actually relax it completely ($V = 0$) or drive it backward ($V < 0$). This may be an appropriate representation of faults for which the transient load is significantly smaller than the accumulated stress or strain at the time the transient is applied (hereafter called "prestress"). It is consistent with estimated magnitudes of triggering dynamic strains that are small relative to assumed failure strain levels (Hill *et al.*, 1993; Anderson *et al.*, 1994; Gomberg and Bodin, 1994; Spudich *et al.*, 1995; Gomberg and Davis, 1996). However, there may be situations in which the prestress is small, and equation (1) should be applied with caution, such as to model deep afterslip, triggered slip, or earthquakes (including aftershocks) on faults that have recently ruptured or that creep. Natural examples of backward slip include observations of left-lateral displacements recorded at several creepmeters on or just adjacent to the creeping section of the San Andreas fault following the Coalinga and Tres Pinos, California, earthquakes (Simpson *et al.*, 1988; Poley *et al.*, 1987). Aftershocks of the 1989 Loma Prieta earthquake indicated both right- and left-lateral slip on faults oriented subparallel to the mainshock fault (Beroza and Zoback, 1993).

Model Experiments

Clock-Advance Hypothesis

In the clock-advance hypothesis, the transient loads simply advance the time of earthquakes that would have happened due to background loading. A principle objection to dynamic earthquake triggering is based on the observation that triggered activity often occurs long after the transient (seismic waves) has passed; we hypothesize and demonstrate that delayed triggering may be explained simply, assuming processes analogous to those in our model occur in nature. The "earthquake cycle" is represented by the time required

for an instability to occur when the system is loaded only by the background velocity, V_b. If a transient causes the instability to occur before completion of the cycle time, the amount of time that it is early is the clock advance. In our clock-advance models, the system is inherently unstable ($k < k_c$) and not initially at steady state under the background load.

In all models, we define the start of the earthquake cycle as the time when both co-seismic and rapid post-seismic slip have ceased. More complex models invoking rate-state constitutive laws begin the cycle with the fault slipping with velocities of ~1 m/sec, typical slip velocities during rupture (Rice and Gu, 1983; Tse and Rice, 1986; Stuart and Tullis, 1995); we choose a later time because this simple slider model lacking inertia cannot simulate dynamic slip rates, nor can ruptures be stopped. However, the results of those more complex modeling studies provide guidance as to the initial conditions appropriate to the start of the earthquake cycle as we define it. In particular, the models of Tse and Rice (1986) (their Figs. 8 and 9) show that when the seismogenic zone has essentially become locked (e.g., at ~4 yr for an 84-yr cycle), the ruptured fault slows to velocities equal to or below the plate velocity (herein V_b), and the stress falls below the steady-state stress at V_b.

Table 1 lists model parameters used in all experiments. Parameters are selected to be representative of geologic, laboratory, or theoretically constrained values such that a cycle duration in the absence of a transient is of the order of hundreds of years under steady background loading. We select transient parameters representative of the duration, frequency content, and amplitudes of seismic waves at regional or remote distances. $V_b = 10^{-10}$ m/sec = 3 mm/yr is comparable to rates of ~8 mm/yr estimated for the Eastern California Shear Zone (Savage *et al.*, 1990), where most of the post-Landers triggering occurred. Laboratory results constrain a, b, and d_c (Dieterich, 1978, 1981; Tullis and Weeks, 1986; Marone *et al.*, 1990; Blanpied *et al.*, 1991; Marone and Kilgore, 1993). In addition to being consistent with these laboratory constraints, specific values of a, b, and d_c used (Table 1) are similar to those used in other earthquake modeling studies [e.g., Sleep (1995) used $a = 0.01$, $b = 0.015$, $d_c = 0.0042$ m; Boatwright and Cocco (1996) used $a = 0.005$, $b = 0.006$, $d_c = 0.001$ m assuming $\sigma = 100$ MPa].

Appropriate values of the critical and material stiffnesses for natural fault systems, and whether they should be constant or time-varying, are highly uncertain. The stiffness is linked to the rupture nucleation process; Dieterich (1986) showed theoretically that a circular slipping fault patch has radius $r = 7\pi G/24\sigma k$ with a critical radius for nucleation at $k = k_c$. While observations and models of rupture nucleation might provide some physical constraint on stiffness values, both the observations and interpretations vary widely [e.g., see Ellsworth and Beroza (1995), Abercrombie and Mori (1994), and references in both]. For example, the numerical models of Deiterich (1992) predict nucleation patch sizes that grow and then shrink as instability is approached and proceeds. The analyses of P-wave onsets by Ellsworth and Beroza (1995) lead them to conclude that critical nucleation patch dimensions scale with the ultimate size of the earthquake, whereas Abercrombie and Mori (1994) conclude that earthquakes nucleate in a cascading process with no systematic dependence on initial patch size. Given these diverse interpretations, and our goal of simply demonstrating qualitatively the feasibility of dynamic triggering as a frictional

Table 1

Sine-Wave + Gaussian, General Gaussian, Ramp, and Gaussian Transients are Described by Equations (9), (13), (14), and (15), Respectively. $\xi(t_0)$ is Set So That the Initial Stress or Friction Equals $\mu(t_0)$. Parameters A, f_0, t_w, and n Determine Transient Characteristics Described by Equation (9).

	a	b	μ_0	d_c(m)	k/k_c	$V_b = V_{ss}$ (m/sec)	V_0(m/sec)	$V(t_0)$ (m/sec)	$\mu(t_0)$	t_w(sec) or V_r	A (cm)	f_0(Hz) or n
Sine-wave + Gaussian (Figs. 2 and 3)	0.005	0.010	0.7	0.001	0.025	10^{-10}	10^{-10}	10^{-10}	0.99 μ_{ss}	400.	60	0.05
Ramp	0.005	0.010	0.7	0.001	0.025	10^{-10}	10^{-10}	10^{-10}	0.99 μ_{ss}	10^{-11} to 10^{-6}	N/A	N/A
General pulse (Fig. 4)	0.005	0.010	0.7	0.001	0.025	10^{-10}	10^{-10}	10^{-10}	0.99 μ_{ss}	400 and 800	50	2, 4 and 2
Sine-wave + Gaussian (Fig. 5)	0.005	0.010	0.7	0.001	1.1	10^{-10}	10^{-10}	10^{-10}	μ_{ss}	400.	0.1	0.05
Gaussian (Fig. 6)	0.005	0.010	0.7	0.001	1.1	10^{-10}	10^{-10}	10^{-10}	0.99 μ_{ss}	400.	0.849, 0.850	2
Gaussian (Fig. 7)	0.005	0.010	0.7	0.001	1.1	10^{-10}	10^{-10}	10^{-10}	0.99 μ_{ss}	200., 400., 800., 1600.	0.850, 0.917, 0.983, 1.050	2

instability process, we assume constant stiffnesses having values consistent with a patch size appropriate to a small earthquake. Our models have a critical patch radius of r_c = 64 m corresponding to a magnitude of $M_L \sim 1$ (Abercrombie and Leary, 1993) [assuming $G = 3.5 \times 10^4$ and using σk_c = 500 MPa/m (equation 7; Table 1) for conditionally stable models]. We also use σk = 12.5 MPa/m (σ = 100 MPa), which is similar to values used in other earthquake modeling studies of σk = 4 MPa/m (Sleep, 1995) or σk = 5 MPa/m (Boatwright and Cocco, 1996). In the numerical study of Roy and Marone (1996), they assumed values of k that are several orders of magnitude larger than ours, but conclude that σk actually must be smaller than even our estimates to be consistent with studies of static or dynamic earthquake triggering.

The sine-wave transient in Figure 2 causes a clock advance, and the instability occurs long after the transient load has finished. Here we simulate seismic waves using a sine wave of frequency f_0, scaled by a Gaussian pulse with amplitude A and width t_w, and functional form

$$x(t)_T = A \sin(2\pi f_0 t) \exp\{-[(t - t_p)/t_w]^2\} \quad -\infty < t < \infty. \quad (9)$$

In this example, the loading cycle starts with the slider moving at the background load velocity, and the shear stress is below the steady-state value [$\mu(t_0) < \mu_{ss}$ and $V(t_0) = V_{ss} = V_b$]. Note that as instability approaches, ξ decreases and V increases. Thus, the transient causes a significant decrease in ξ and hastens the time of instability. In these models, generation of clock advances of tens of days or more require transient amplitudes that exceed those likely from seismic waves by about an order of magnitude; in our models, A is of the order of several tens of centimeters. According to the standard formula for surface-wave magnitude,

$$M_s = \log A_{20} + 2.0 + 1.66 \log \Delta, \quad (10)$$

the amplitude of a 20-sec-period surface wave at distance $\Delta \sim 15°$ from an $M_s \sim 7.5$ earthquake equals $A_{20} \sim 0.4$ cm. Assuming the same distance dependence as equation (10), $A_{20} \sim 10$ cm would be expected at a distance of several hundred kilometers. Although better agreement would clearly be more satisfying, these simple models are not meant to account for the true complexity of nature and thus should be interpreted heuristically and qualitatively. Indeed, the system response varies depending on the values of parameters used in our simple slider model, on effects not included such as inertia (Roy and Marone, 1996), and for alternative representations of faulting [e.g., the slab model of Campillo *et al.* (1996)].

Sine-wave transients always produce clock advances, as opposed to clock retardations, as long as the signal contains several nearly symmetric oscillations. This result seems contrary to intuition, which might predict that a purely symmetric oscillatory load should have no net affect (i.e., the load increases are canceled by the decreases). The fact that this does not occur arises from the evolutionary nature implicit in rate-state models (i.e., the response depends on the history of the loading) and the fact that V remains positive, implying that the transients do not drop the stress to zero or below. We clarify this by showing the system response to the oscillatory load of Figure 2a in greater detail (Fig. 2b). The sharp positive increases in slider velocity may be understood more easily by rewriting equation (1) as

$$V = V_0 \exp\{[\mu - \mu 0 + b \ln(\xi V_0/dc)]/a\}. \quad (11a)$$

Therefore, the change in V from t_1 to $t_2 = t_1 + \Delta t$ is

$$V(t_2) = V(t_1) \exp\{\Delta\mu/a\} [\xi(t_2)/\xi(t_1)]^{b/a}, \quad (11b)$$

and we see that slider velocity depends exponentially on changes in the frictional coefficient, $\Delta\mu = \mu(t_2) - \mu(t_1)$. From equation (3), the change in friction or shear stress is proportional to the load-point velocity relative to that of the slider:

$$\Delta\mu \sim d\mu/dt\, \Delta t = k[dx_{lp}/dt - V]\, \Delta t. \quad (12)$$

Thus, as shown in Figure 2b, the slider velocity exponentially increases during the half-cycle when $dx_{lp}/dt - V > 0$ and decreases when $dx_{lp}/dt - V < 0$; this corresponds to net forward and backward loading, respectively. During a half-cycle $\Delta\mu > 0$, V increases exponentially so $d\xi/dt \sim -\xi V/dc$ and the state variable decreases approximately exponentially. During the other half-cycle $\Delta\mu < 0$, V decreases exponentially, and $d\xi/dt$ is bounded at a value of 1 (equation 2) so that the state variable increases negligibly. Thus, the net change in each cycle is a decrease in ξ, which brings the system closer to the earthquake. Although not likely for seismic waves, model experiments show that clock retardations may result from asymmetric loads in which negative time segments sufficiently exceed the positive ones in amplitude and/or duration.

We use the model to test assumptions about the role of prestress in triggering and also to gain new insight into the meaning and implications of clock advances. The great distance between locations of triggered seismicity and the Landers earthquake, and thus small associated stress or strain changes, led to the suggestion that faults at these sites were prestressed to near-failure levels (Hill *et al.*, 1993). Use of clock-advance estimates in assessing probabilities of future earthquakes requires assumptions about prestress and failure stress levels (Stein *et al.*, 1992; King *et al.*, 1994; Harris and Simpson, 1995). We examine the dependence of dynamic triggering on prestress by modeling the response to transients with identical characteristics occurring at different times in the loading cycle; the background load increases with time so that later transient load times are equivalent to greater prestress. Results (Fig. 3) for the initial conditions and transient of Figure 2 support the suggestion that the triggered seismicity depends on prestress and that faults that

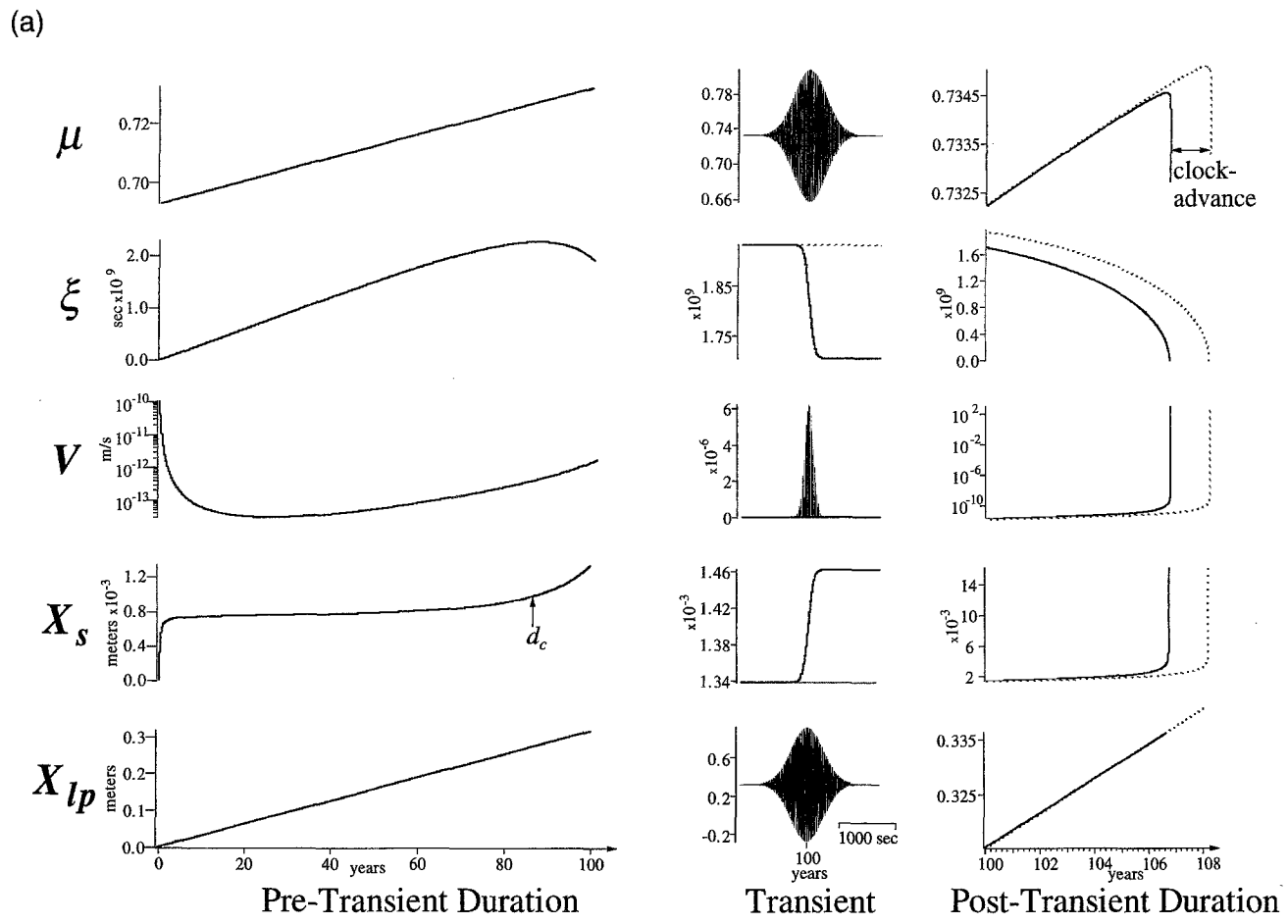

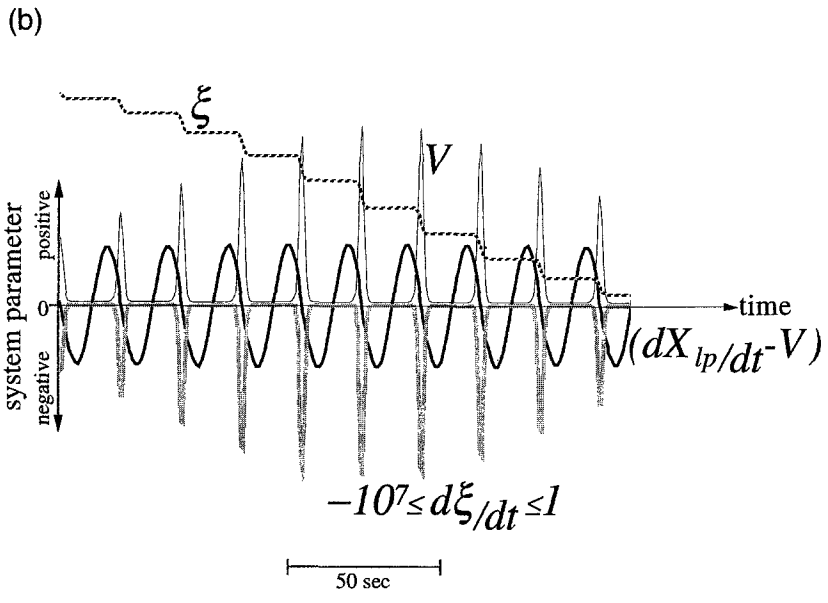

Figure 2. (a) Evolution of the spring-slider variables from the start of the loading cycle ($t = 0$) until instability [$t \sim 106.6$ and 108.1 yr for systems loaded with both a transient plus a background (solid curves) and with a background only (dotted curves), respectively]. Note that fault strengthening dominates initially such that ξ increases and V decreases with time. Once the slider displacement, X_s, reaches the critical slip distance, d_c, slip-dependent weakening dominates so that ξ begins to decrease, enabling instability ultimately to occur. A clock advance refers to the amount of time that the transient hastens instability, primarily by causing a significant decrease in ξ relative to its evolution for a background load only (center panel). Note the time scales change for the durations prior to, during, and after the transient. All dependent variable axes are linear except for V prior to and after the transient. (b) Temporally expanded view of the transient in (a), centered at the peak of the transient. Note that during the half-cycle when $d\mu/dt = k(dx_{lp}/dt - V) > 0$, $d\xi/dt \sim -\xi V/dc$ so that ξ decreases approximately exponentially and V exponentially increases. During the half-cycle when $d\mu/dt < 0$, corresponding to backward loading, $d\xi/dt$ is bounded at a value of 1 so that the state variable increases negligibly and V decreases exponentially. Thus, after each transient cycle, ξ decreases, thus hastening instability.

failed sooner after Landers were prestressed closer to failure. The results also show that the triggering delay does not scale linearly with the level of prestress. (A smaller delay should mean a greater potential for recognizable triggering.) Albeit not an exhaustive search of the range of possible models, other numerical experiments assuming different initial conditions [e.g., $\mu(t_0) = \mu_{ss}$ and $V(t_0) < V_{ss} = V_b$] and/or model parameters yield comparable results.

We explore the frequency and rate dependence further using a constant rate or ramp and general pulse loading functions. The latter has functional form

$$x(t)_T = A \exp\{-[(t - t_p)/t_w]^n\} \tag{13}$$

in which n is some even integer. The pulse has amplitude, A, and width, t_w. Physically, this approximates a body wave, which may not have zero mean. The response to this load function is qualitatively the same as for the oscillatory signals described by equation (9); we use this pulse function because the relationship between the time and frequency domains is simpler. As seen below, use of a simply characterized function facilitates sensitivity tests and understanding of the system response in both temporal and frequency domains. A ramp function

$$\begin{aligned} x(t)_T &= 0 & t < t_s \\ &= V_r(t - t_s) & t \geq t_s \end{aligned} \tag{14}$$

simulates loading at a constant rate, V_r, starting at some time t_s, which might represent strains associated with extraction or injection of fluid or gas (Gomberg and Davis, 1996), perhaps magma intrusion (Rydelek *et al.*, 1992), or loading of a small fault by a larger nearby fault that is creeping (Dieterich, 1993). We hypothesize that more rapidly applied transients will more readily cause instabilities. This is physically reasonable if considered in the context of ξ representing contact time. The slower the slip velocity, the larger, older, and stronger the new population of contacts will be, and thus rupture will be more difficult (Dieterich, 1979). We find that for models that differ only in the value of V_r used (Table 1), the clock advance increases nonlinearly with increased loading velocity. For example, when $t_s = 100$ yr for $V_r = 10^{-6}$, 10^{-8}, and 10^{-10} m/sec, instability occurs after 0.01, 0.55, and 6.35 yr, respectively (corresponding to clock advances of 8.05, 7.2, and 1.71 yr, respectively). The observation that instability occurs when V reaches approximately the same value for different ramp velocities might suggest that instability occurs when V exceeds some critical level and therefore that a rate-state constitutive law is not required. However, some mechanism must cause the slider to accelerate far beyond the loading velocity (become unstable). A response governed by rate-state laws is one way to accomplish this while also requiring excedance of a critical threshold for instability.

Experiments with transient pulse loads indicate that the potential for triggering depends on both the loading rate, dx_{lp}/dt, and the duration, t_w. We explore this dependence by comparing clock advances for pulses rising and falling with varying rates (different powers of the exponential in equation 13) and having different durations (different values of t_w). Because the ramp and pulse models differ only in the transient load, the net slip prior to the transient nearly equals that of the ramp load, $\sim 1.34 \times 10^{-3}$ m. The net slip at instability is $\sim 1.6 \times 10^{-2}$ m and nearly identical to that for the ramp models. Again, this is not surprising given that both types of models have identical constitutive parameters governing their response. In terms of real earthquakes, the shorter, more rapidly varying (higher frequency) transients might represent closer, smaller earthquakes, and longer, more slowly varying (lower frequency) transients might represent larger, more remote earthquakes. Pulses of equal duration (identical values of t_w) but that rise and fall more quickly lead to greater clock advances (e.g., the $n = 4$ vs. the $n = 2$ "small earthquake" pulses in Fig. 4). However, the increase in clock advance associated with increased load rate may be compensated for by the decrease in duration of a narrower, steeper-sided pulse (e.g., the $n = 4$, $t_w = 400$ "small, close, high-frequency earthquake" vs. the $n = 2$, $t_w = 800$ "large, distant, earthquake" pulses in Fig. 4).

The results presented in Figure 4 suggest that a transient load applied more slowly but lasting longer may cause a larger perturbation to the system. More generally, the results indicate trade-offs between transient characteristics, such as frequency content and duration, and their potential to trigger instabilities. We suggest that the latter is simply related to the ability of each characteristic to induce slip on the slider surface. Viewing the evolution of state, ξ, as the competition between its time dependence and the product of the slider slip, x_s, and velocity, $V = dx_s/dt$, leads us to this suggestion. Mathematically, the evolution of $\xi(x_s, t)$ may be described by

$$\frac{d\xi}{dt} = \frac{\partial \xi}{\partial t} + \frac{\partial \xi}{\partial x_s}\frac{\partial x_s}{\partial t} \tag{15a}$$

or

$$\frac{d\xi}{dt} = \frac{\partial \xi}{\partial t} + \frac{\partial \xi}{\partial x_s} V. \tag{15b}$$

This time-slip competition becomes explicit by comparing equation (15b) with the evolution equation (2); it follows that

$$\frac{\partial \xi}{\partial t} = 1 \quad \text{and} \quad \frac{\partial \xi}{\partial x_s} = -\frac{\xi}{d_c}. \tag{16}$$

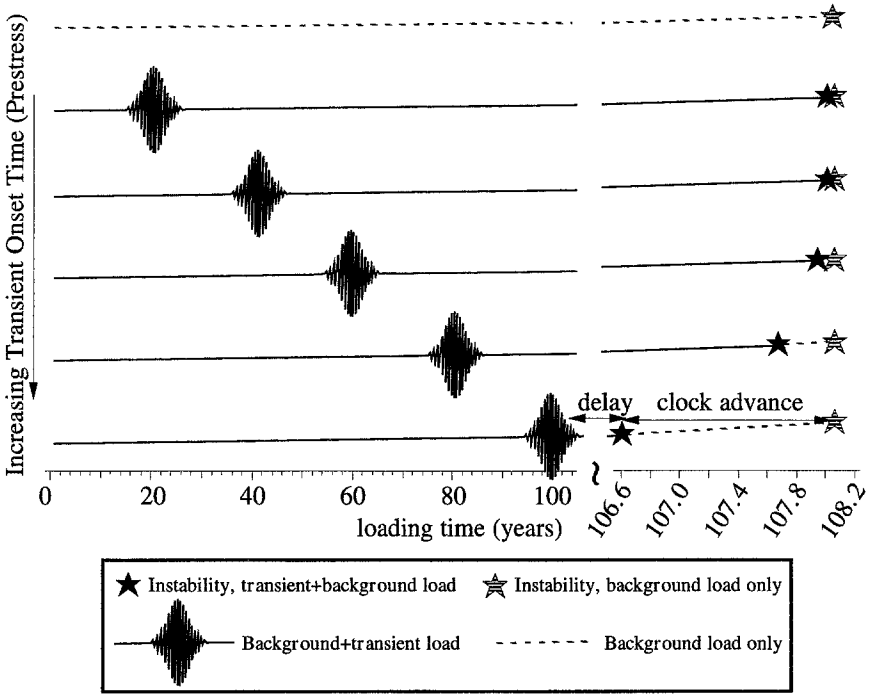

Figure 3. Drawing illustrating the nonlinear affect of the time, or equivalently the prestress, when the transient load is applied on the timing of instability. Each row represents a different calculation in which only the time of the transient differs from the other rows. The bottom trace illustrates schematically the results shown in Figure 2a. The "delay" refers to the time difference between the transient and instability, and the "clock advance" refers to the time difference between instabilities with and without the transient load. The gap in each trace indicates a change in plotting time scales.

Thus, time causes ξ to increase, making faults stronger, but the slip dependence is negative, competing against the work of time and making faults weaker. For equal time intervals, the transient that induces the greater slip will be most effective at weakening the fault, thereby causing it to fail sooner. The response to the three transients of Figure 4 demonstrate this. As the slider slip increases (by 1.05×10^{-4}, 2.20×10^{-4}, to 2.37×10^{-4} m corresponding to transients with $n = 2$ and $t_w = 400$, $n = 4$ and $t_w = 400$, and $n = 2$ and $t_w = 800$), so do the corresponding clock advances (447, 888, and 936 days, respectively). These slip increases occur during equal time intervals (± 1000 sec from the transient peaks).

New Seismicity Hypothesis

The above models assume that an instability or earthquake is inevitable, the transient simply shortens the time to its occurrence. An alternative is that the transient load actually changes an otherwise stable system, such that the transient is the primary cause of the triggered earthquake. This hypothesis, that triggered earthquakes might not have happened in the absence of the triggering earthquake, need not violate distant boundary conditions such as the slip or strain energy budget imposed by plate motions. "New" triggered seismicity simply requires a change in the partitioning of strain relaxation between aseismic and seismic processes. Moreover, this change need not be large, as most triggered earthquakes seem to be small-magnitude events. Evidence from triggered seismicity following the Landers earthquake at Long Valley, California (Hill *et al.*, 1995), and at The Geysers, California, for many remote earthquakes (Gomberg and Davis, 1996) suggests that triggered activity occurs in excess of the background seismicity.

We investigate this alternative hypothesis and the existence and frequency dependence of a critical triggering threshold. Both laboratory and field data indicate that for triggering to occur a critical loading threshold must be exceeded. This appears true whether the load is static or transient. Moreover, field data suggest that this threshold is frequency dependent (Anderson *et al.*, 1994; Gomberg and Davis, 1996), although the precise form of the dependency remains unclear. Not surprisingly, the model calculations demonstrate that a transient load can easily cause an otherwise stable system to become unstable. We model stable systems in two ways. In both models, we chose $b > a$ and $V(t_0) = V_{ss} = V_b$. In the first model, $k < k_c$, so that it is inherently unstable (Ruina, 1983) except when the system is initially at steady state [$\mu(t_0) = \mu_{ss}$]. We acknowledge that such conditions may be difficult to achieve over large spatial or temporal scales in the real Earth but suggest that they may

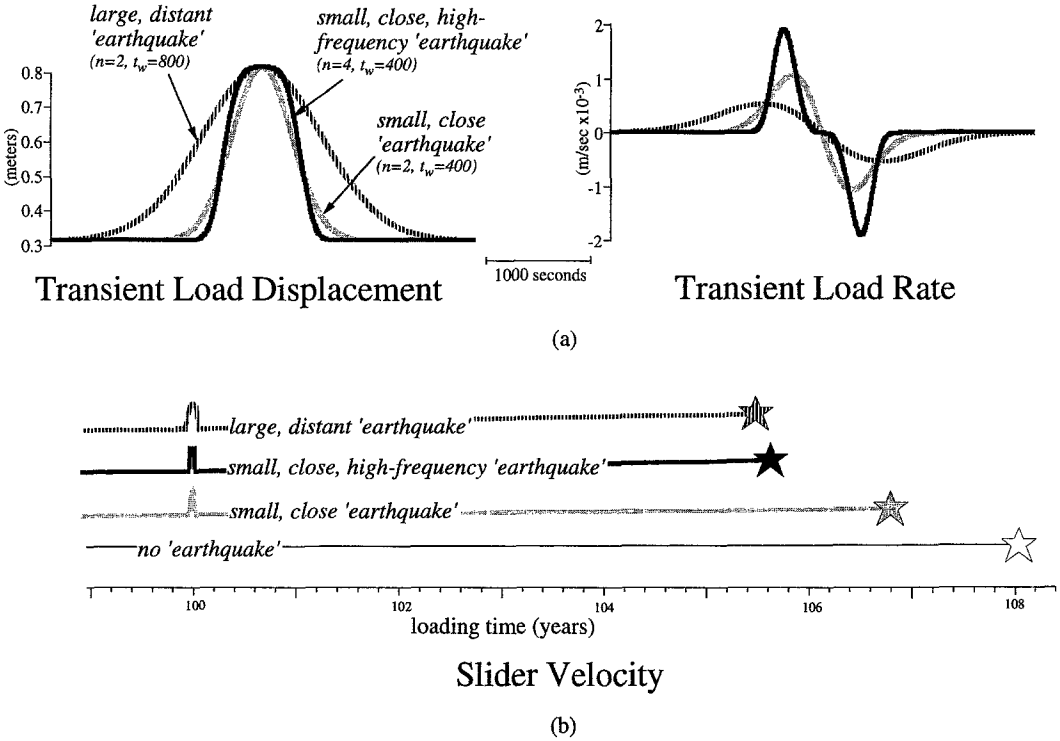

Figure 4. Top: Transient load pulses that qualitatively represent the effect of seismic waves associated with a large distant earthquake (striped curves), and two small, close earthquakes that differ in their frequency content (solid and shaded curves). Although these have identical peak displacement amplitudes (left), their associated loading rates differ (right). Bottom: Schematic of the slider velocity V evolution for the three transient loads above (all have identical background loads). Of the loads from the two small, close earthquakes, instability occurs sooner for the one with a more rapid loading rate, or equivalently more energy at higher frequencies. However, the clock advance also appears to depends on load duration, as illustrated by the even larger clock advance associated with the load from the large, distant earthquake even though it has the slowest loading rate.

on smaller, yet adequate, scales be significant. Laboratory experiments show that the parameters that determine stability can change as the system evolves (Dieterich, 1981; Wong *et al.,* 1992), perhaps making these steady-state conditions possible. [This also suggests another hypothesis for generating new earthquakes, one in which an initially stable system becomes unstable due to changing system parameters. We have not attempted to model such systems, as it would add degrees of freedom (largely unconstrained) and computational complexity to our simple models, possibly obscuring their fundamental behavior.] The second considered model is conditionally stable. In this case, $k > k_c$, and instability occurs only if a sufficiently large load perturbs the system variables V, ξ, and μ to an unstable condition.

In the inherently unstable model ($k < k_c$), extremely small transient amplitudes (orders of magnitude less than d_c) perturb the system from steady state allowing the background load to then bring it to instability in a relatively short time. Consideration of the state of the system at the time the system is perturbed from stability clarifies the reason for this behavior. Note that clock-advance models begin in an unstable state but with no net slip so that initially strengthening occurs (see Fig. 2a); ξ increases and V decreases by several orders of magnitude (the "direct effect"). At this low velocity, it then takes many tens of years (~85 for the model in Fig. 2) for the slip to equal d_c and weakening to commence. In the initially stable system (Fig. 5), V differs only slightly from $V_{ss} = V_b$, and the slip already far exceeds d_c. The slider surface does not strengthen (i.e., there is no "direct effect"), ξ never increases, and V never decreases. Thus, the system rapidly accelerates to instability. As in the clock-advance models, the time to instability from the transient decreases with increased transient amplitude. Not surprisingly, there is no dependence on when the transient is applied because system parameters remain at their steady-state values until the transient is applied.

In the conditionally stable model ($k > k_c$) with initial shear stresses at or below steady-state values, the timing of instability does not depend on when the transient is applied. In this model, instability occurs either during the transient or, below some threshold amplitude, not at all. We attribute this lack of significant delay to the large stiffness that implies

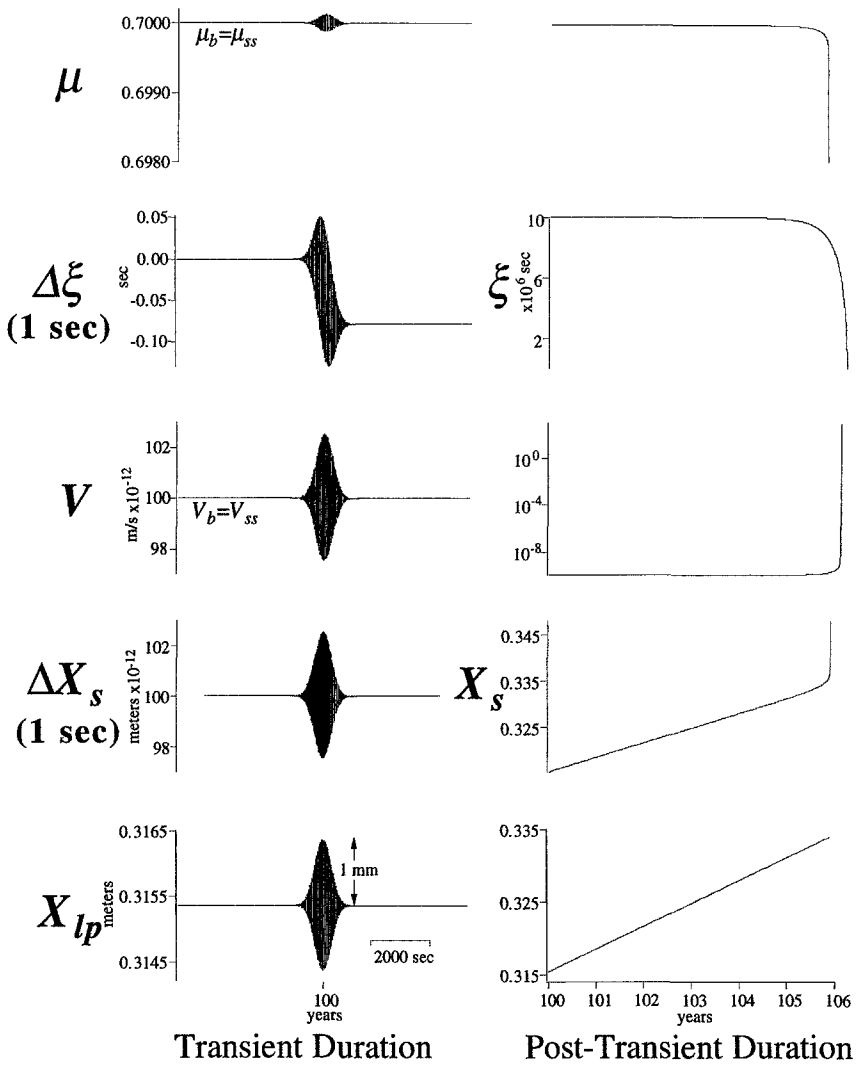

Figure 5. Evolution of the spring-slider variables from 4000 sec before the transient peak (at $t = 100$ yr) until instability at $t \sim 105.9$ yr. Prior to the times shown, all variables have the same steady-state values as those plotted before the transient. We show the changes in state, ξ, and slider displacement, X_s (Δs in the labels indicate incremental changes) in 1-sec increments because they would not be resolvable on a plot of the absolute values. Although these changes are many orders of magnitude smaller than the absolute steady-state value of ξ, they are sufficient to perturb ξ and enable instability to ultimately occur. Note that the vertical scales for μ for both durations are identical, and for V, they are linear and logarithmic for the earlier and later durations, respectively.

a rapidly changing shear stress (equation 4); i.e., once the perturbation is sufficiently large, the system rapidly accelerates to instability. Transients below some threshold cause system variables to exhibit damped oscillations that quickly reach steady-state values (Rice and Gu, 1983).

The conditionally stable model exhibits a critical threshold for triggering instability. [Definition of a threshold for the other models ($k < k_c$) is impossible because the slightest perturbation from steady state leads to instability, albeit with possibly long time delay.] Figure 6 compares the evolution of system variables for Gaussian pulse loads just above and below the threshold. This type of transient enables us to explore easily the rate or frequency dependence of the transient load threshold amplitude for the conditionally stable model. For a given Gaussian pulse load of amplitude A centered at time t_p with functional form

$$x(t)_T = A \exp\{-[(t - t_p)/t_w]^2\} \tag{17}$$

and width, tw, a threshold may be estimated by running the model calculations iteratively, decreasing and increasing the amplitude until two adjacent values do and do not trigger an instability. We select a Gaussian because of the simple an-

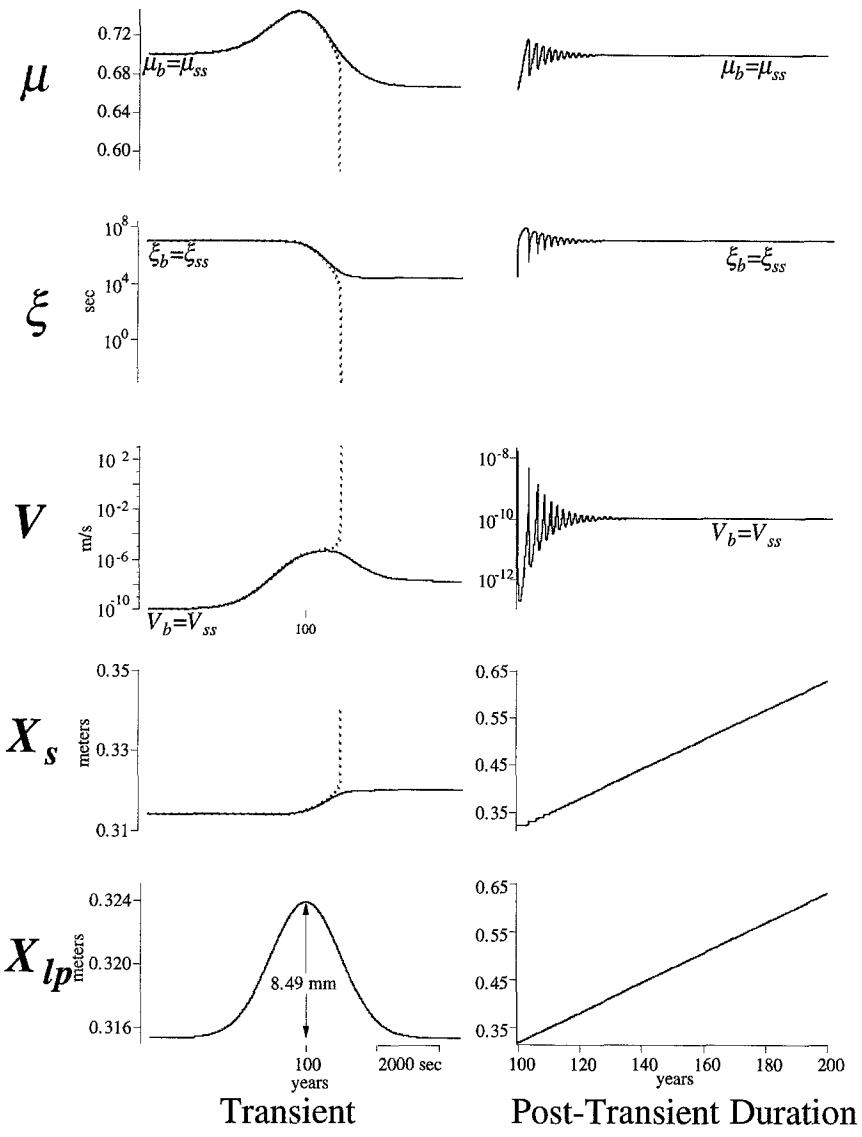

Figure 6. Evolution of the spring-slider variables for transient loads just above (A = 8.50 mm, dotted curve) and below (A = 8.49 mm, solid curve) the triggering threshold for this pulse shape. We plot the durations ±4000 sec around the transient peak (at t = 100 yr) and for 100 yr after the transient. Prior to the times shown, all variables have the same steady-state values as those plotted before the transient. After the transient that is below the threshold, variables exhibit damped oscillations until they return to their steady-state values, as predicted by Rice and Gu (1983). Note that the vertical scales for μ and ξ for both durations are identical.

alytic relationship between its time-domain representation and its amplitude spectrum:

$$A \exp\{-[(t - t_p)/t_w]^2\} \rightarrow A\, t_w \exp[-(\pi f t_w)^2], \quad (18)$$

where f is frequency and the arrow implies transformation to spectral amplitude. Thus, a wider pulse with equal amplitude to a narrower one will be relatively enriched in low frequencies and depleted in high frequencies. Figure 7 shows that a large increase in transient duration is required to compensate for a small decrease in amplitude. In the frequency domain, this implies that loads relatively enriched in higher frequencies trigger instabilities more easily. Roy and Marone (1996) and Gomberg and Davis (1996) make similar inferences based on numerical models and field observations, respectively.

Note that for these new-seismicity models, the transient (sine-wave Gaussians, equation 9, and general pulses, equation 13) amplitudes required to cause instability are much smaller than those of the clock-advance models and are consistent with amplitudes that might arise from seismic waves. While it is tempting to interpret this as indicating that triggered seismicity more probably represents new earthquakes

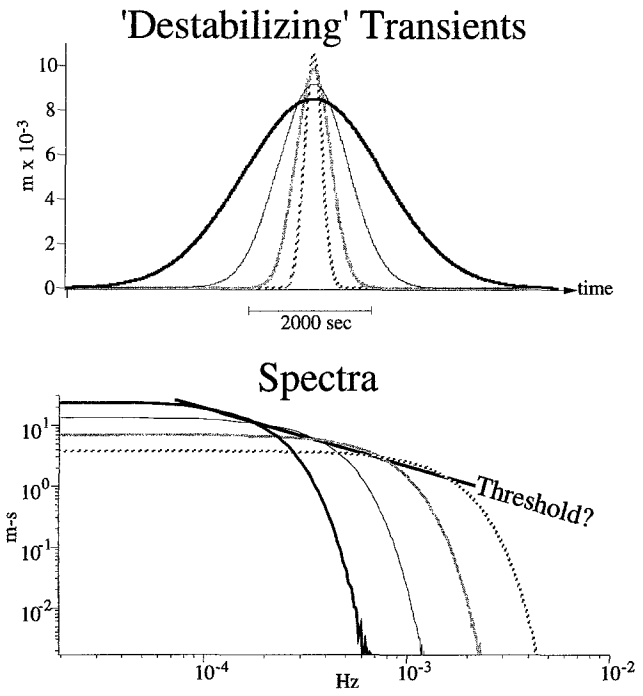

Figure 7. Top: Gaussian load displacements calculated according to equation (15) that just exceed a triggering threshold for conditionally stable models (Table 1 lists model and triggering transient characteristics; nontriggering amplitudes are 0.01 mm smaller). Bottom: Amplitude spectra corresponding to the transient loads above, coded by line type. The simplest threshold, i.e., a function exceeded by all spectra at some frequency, is shown by the thick straight line (corresponds to $1/f$).

rather than earthquakes advanced in time, we again caution against such quantitative interpretation of results from such simple models.

Discussion

We emphasize again that these simple models cannot fully represent the complexity of real seismic wave trains or of the processes that lead to earthquake rupture, and thus, they do not enable us to make quantitative interpretations or predictions. Nonetheless, they do provide a framework for understanding how triggered seismicity may be caused by seismic waves emanating from earthquakes at very remote distances. Regardless of our ability to quantitatively model the underlying mechanism, the plausibility of remote dynamic triggering is demonstrated by the real-world observations of remotely triggered seismicity, particularly those following the Landers earthquake (Hill *et al.*, 1993; Gomberg, 1996) and at The Geysers, California (Stark and Davis, 1996; Gomberg and Davis, 1996). Having demonstrated that the delays between the transient seismic strains and triggered seismicity may be plausibly explained, one might readily accept that the seismic waves from nearby earthquakes could trigger nearby seismicity yet still may find very remote triggering intuitively problematic. Our results (Fig. 4) indicate that the seismic strains from the distant earthquake can have a greater potential to advance the clock than do those from a nearby event with seismic strains of comparable amplitude. If we let the short-duration transient load represent a close, small earthquake and the long-duration transient a distant, larger earthquake, a back-of-the-envelope calculation indicates that the distant earthquake need not be exceedingly large for remote triggering to be viable. At a particular frequency, the seismic strain amplitude for a distant, large earthquake of scalar moment M_{0f} at a distance X_f will be approximately proportional to

$$(M_{0_f}/X_f^{\gamma}) \exp^{(-2\pi X_f/2CTQ)} \tag{19}$$

in which C is the phase velocity, Q is the quality factor, T is the period, and γ is the spreading coefficient ($\gamma \sim \frac{1}{2}$ for surface waves). Assuming a standard moment-magnitude relation

$$M_w = 2/3 \log M_0 - 10.7 \tag{20}$$

(Hanks and Kanamori, 1979), $C \sim \pi$, and neglecting radiation pattern and source spectral difference, then for the waves from a large, distant earthquake to have the same amplitude as those from a smaller one at closer distance X_c, the magnitude difference between the two would be

$$Mw_f - Mw_c \approx 2\gamma/3 \log(X_f/X_c) + \frac{2(X_f - X_c)}{3TQ\ln(10)}. \tag{21a}$$

Supposing $X_f \sim 1000$ km and $X_c \sim 10$ km, $\gamma \sim \frac{1}{2}$, this equals

$$Mw_f - Mw_c \approx \frac{2}{3} + \frac{289}{TQ}, \tag{21b}$$

which is less than 2 to 3 magnitude units assuming typical Q values, greater than several 100, and periods longer than a few seconds. A similar calculation using the standard definition for surface-wave magnitude (Gutenberg, 1945) yields

$$Ms_f - Ms_c \approx 1.66 \log(X_f/X_c), \tag{22}$$

again showing that an earthquake several orders of magnitude farther away need only be ~3 magnitude units larger to have a similar, if not greater, triggering potential.

The effects of both static and dynamic changes are not easily predictable, among other things, depending on the generally unknowable characteristic of how far along a fault is in its earthquake cycle. Dieterich (1992) reached similar conclusions, modeling the stability of a finite fault using interacting fault patches, the same constitutive relations, and specifying some initial load (i.e., prestress) and constant load rate. At nonzero loading rates, Dieterich (1992) found that

the time to failure increased nonlinearly (logarithmically) as the prestress level and/or the load rate decreased. The nonlinear and rate-dependent relationship between load and instability suggests that, assuming dynamic triggering was in part responsible, the post-Landers seismicity increase may be anomalous only in its large spatial extent. If delayed triggered events and/or remote triggering are possible, then remotely triggered earthquakes may occur at some level all the time, yet would be difficult to associate with the causative event. This may also explain the apparent lack of tidal triggering when searched for as a modulation in seismicity rates (Heaton, 1982; Rydelek *et al.,* 1992). Dieterich (1987) applied a rate-state model to examine tidal triggering, or equivalently the modulation of seismicity rates by sinusoidal loading. He found, as we have for transient loading, that only for sufficiently large sinusoid amplitudes is instability nearly instantaneous and rate modulation detectable. His quantitative estimates indicate that except at low normal stresses, instabilities triggered by tidal loads may have delays that obscure any periodic modulation.

There exists growing observational evidence that extremely small (relative to earthquake stress/strain drops) static or dynamic stress/strain changes affect seismicity rates during aftershock sequences (Reasenberg and Simpson, 1992) and affect the probability of moderate to large earthquakes (Harris and Simpson, 1992; Jaume and Sykes, 1992, 1996; Stein *et al.,* 1992; Du and Aydin, 1993; King *et al.,* 1994; Harris and Simpson, 1995). The results described herein suggest that the effectiveness of such small changes may be understood when one considers what is sufficient to initiate instabilities. Moreover, the rate dependence of this instability model suggests that the rate at which these changes occur is a key characteristic in their effectiveness. More rapid or high-frequency transients are more effective triggers. In the clock-advance models, the greater the prestress, the shorter the delay between triggering and triggered events. This leads us to suggest that aftershocks may be easily and immediately triggered by small stress/strain changes because the prestress must be high (or the mainshock would not have occurred). Co-seismic static changes may be especially effective at immediately triggering aftershocks, perhaps more so than dynamic stresses/strains, because the static changes occur nearly instantaneously.

Conclusions

We have tested various hypotheses related to the triggering of seismicity by transient stress/strain changes, i.e., changes associated with seismic waves from near and distant earthquakes. The relative recency of the recognition that such triggering may be possible, and thus, little prior work on the subject, led us to begin by posing simple hypotheses and testing them with simple qualitative models. Our basic assumption is that earthquake triggering is a stick-slip process. Thus, we studied the potential for, and characteristics of, fault instabilities using a simple spring-slider model and rate-state constitutive laws.

In the first hypothesis studied, transients simply hasten the time of earthquakes that ultimately would have happened due to constant background loading alone. We demonstrate that transient loads can trigger delayed instabilities with significant clock advances. Although the model system is very simple, these clock-advance models predict complex relationships between the triggering delays, the clock advances, and the transient characteristics. The delays and clock advances depend nonlinearly on when in the loading cycle the transient load is applied. We interpret this as implying that the potential for faults to fail does not grow linearly with time from the start of the earthquake cycle, even when loaded at a constant background rate. The timing of instability also appears to depend strongly and nonlinearly on the loading rate, with faster loading rates more rapidly hastening instability. This may imply that seismic waves containing greater amounts of high-frequency energy more effectively trigger seismicity. However, results also show that the transient duration significantly influences the clock advance. Close (tens of kilometers) small or moderate earthquakes and remote (thousands of kilometers) earthquakes 2 to 3 magnitude units larger may be equally as effective at triggering seismicity.

Our second suite of model calculations tests the hypothesis that triggered seismicity represents earthquakes that would not have happened without the transient load. This still satisfies regional strain energy budgets, requiring only alteration of the partitioning between seismic and aseismic deformation. Such alteration will be minor if triggered earthquakes are small to moderate in magnitude. We test this hypothesis using two new-seismicity models: (1) ones that are inherently unstable but slide at steady-state conditions under the background load and (2) others that are conditionally stable such that a stability boundary must be crossed by a sufficiently large perturbation for instability to occur. Very small amplitude transients, relative to the clock-advance models, appear able to trigger instability in both types of new-seismicity models studied. The unstable steady-state models predict delayed instability with the delay depending inversely and nonlinearly on the transient amplitude (like in the clock-advance models). Although we have not done an exhaustive search of possible models, we were unable to generate delayed triggering with the conditionally stable models (instability always occurred during the transient). For both of these new-seismicity models, the potential for triggering is independent of the time, or equivalently the prestress state, when the transient load is applied (unlike the clock-advance models). Finally, we explore the characteristics of a critical triggering threshold using a series of simple pulses with differing spectral characteristics. The results are generally consistent with a spectral amplitude threshold that is inversely proportional to frequency.

In short, we have demonstrated qualitatively that frictional instability theory provides a context to explain how

transient stresses or strains may trigger seismicity. Thus far, we have modeled only a single "characteristic" earthquake. A next step is to examine how our results scale to the dynamic triggering of multiple earthquakes on fault systems; i.e., how it might alter seismicity rates on a variety of spatial and temporal scales. The challenge now is to begin developing more sophisticated models that will enable quantitative testable predictions about the change in seismicity rates due to dynamic triggering and threshold triggering slip values and their associated clock advances. This should be possible with further analysis of the rate and state equations, combined with additional seismologic information. Specifically, with respect to the former, analytic relations may be derived describing the change in fault slip and potential for triggering (assuming a critical slip distance) with the triggering earthquake's signal duration and moment and the triggered fault prestress (or slip rate at the time of the transient) (Sleep, personal comm., 1996). These need to be constrained by seismologic or geologic information about the statistics of potentially triggering earthquakes, fault slip rates and prestress, and seismic-wave characteristics. Trade-offs between triggering earthquake distance and magnitude and constitutive parameters on these predictions also may be quantified. Of equal import, we also must begin to identify observations that will distinguish between the various qualitative, yet distinctly different, model predictions described herein.

Acknowledgments

We thank Fabrice Cotton, Joe Andrews, and David Hill for their thorough reviews and thought-provoking questions and comments. We especially thank Norm Sleep not only for his thorough review but also for discussions about future enhancements to this work. This manuscript is CERI Contribution No. 308.

References

Abercrombie, R. and P. Leary (1993). Source parameters of small earthquakes recorded at 2.5 km depth, Cajon Pass, southern California: implications for earthquake scaling, *Geophys. Res. Lett.* **20,** 1511–1514.

Abercrombie, R. and J. Mori (1994). Local observations of the onset of a large earthquake: 28 June 1992 Landers earthquake, *Bull. Seism. Soc. Am.* **84,** 725–734.

Anderson, J. G., J. N. Brune, J. N. Louie, Y. Zeng, M. Savage, G. Yu, Q. Chen, and D. dePolo (1994). Seismicity in the western Great Basin apparently triggered by the Landers, California, earthquake, 28 June 1992, *Bull. Seism. Soc. Am.* **84,** 863–891.

Beroza, G. C. and M. D. Zoback (1993). Mechanism diversity of the Loma Prieta aftershocks and the mechanics of mainshock-aftershock interaction, *Science* **259,** 210–213.

Bodin, P. and R. Bilham (1994). 3D geometry of the strain-field at transform plate boundaries: implications for seismic rupture, *Geophys. Res. Lett.* **21,** 2523–2526.

Blanpied, M. L., D. A. Lockner, and J. D. Byerlee (1991). Fault stability inferred from granite sliding experiments at hydrothermal conditions, *Geophys. Res. Lett.* **18,** 609–612.

Boatwright, J. and M. Cocco (1996). Frictional constraints on crustal faulting, *J. Geophys. Res.* **101,** 13895–13910.

Campillo, M., I. R. Ionescu, J. C. Paumier, and Y. Renard (1996). On the dynamic sliding with friction of a rigid block and of an infinite elastic slab, *Phys. Earth Planet. Interiors* **96,** 15–23.

Carlson, J. M. and J. S. Langer (1989). Mechanical model of an earthquake, *Phys. Rev. A* **40,** 6470–6484.

Carlson, J. M., J. S. Langer, B. Shaw, and C. Tang (1991). Intrinsic properties of a Burridge–Knopoff model of a fault, *Phys. Rev. A* **44,** 884–897.

Das, S. and C. H. Scholz (1981). Off-fault aftershock clusters caused by shear stress increase?, *Bull. Seism. Soc. Am.* **71,** 1669–1675.

Dieterich, J. H. (1978). Time dependent friction and the mechanisms of stick slip, *Pure Appl. Geophys.* **116,** 790–806.

Dieterich, J. H. (1979). Modeling of rock friction 1. Experimental results and constitutive equations, *J. Geophys. Res.* **84,** 2161–2168.

Dieterich, J. H. (1981). Constitutive properties of faults with simulated gouge, *Am. Geophys. Union Geophysical Monograph* **24,** 103–120.

Dieterich, J. H. (1986). A model for the nucleation of earthquake slip, in *Earthquake Source Mechanics,* S. Das, J. Boatwright, and C. Scholz (Editors), American Geophysical Monograph 37, 36–49.

Dieterich, J. A. (1987). Nucleation and triggering of earthquake slip: effect of periodic stress, *Tectonophysics* **144,** 127–139.

Dieterich, J. A. (1992). Earthquake nucleation on faults with rate- and state-dependent strength, *Tectonophysics* **211,** 115–134.

Dietrerich, J. (1993). Simulation of earthquake triggering, *EOS* **74,** 317–318.

Dietrerich, J. (1994). A constitutive law for rate of earthquake production and its application to earthquake clustering, *J. Geophys. Res.* **99,** 2601–2618.

Dietrerich, J. and B. Kilgore (1996). Implications of fault constitutive properties for earthquake prediction, *Proc. Natl. Acad. Sci.* **93,** 3787–3794.

Dodge, D. A., G. C. Beroza, and W. L. Ellsworth (1995). Foreshock sequence of the 1992 Landers, California, earthquake and its implications for earthquake nucleation, *J. Geophys. Res.* **100,** 9865–9880.

Du, Y. and A. Aydin (1993). Stress transfer during three sequential moderate earthquakes along the central Calavera fault, California, *J. Geophys. Res.* **98,** 9947–9962.

Ellsworth, W. L. and G. C. Beroza (1995). Seismic evidence for an earthquake nucleation phase, *Science* **268,** 851–854.

Gomberg, J. (1996). Stress/strain changes and triggered seismicity following the Mw7.3 Landers, California, earthquake, *J. Geophys. Res.* **101,** 751–764.

Gomberg, J. and P. Bodin (1994). Triggering of the M_s = 5.4 Little Skull Mountain, Nevada, earthquake with dynamic strains, *Bull. Seism. Soc. Am.* **84,** 844–853.

Gomberg, J. and S. Davis (1996). Stress/strain changes and triggered seismicity at The Geysers, California, *J. Geophys. Res.* **101,** 733–750.

Gu, J., J. R. Rice, A. L. Ruina, S. T. Tse (1984). Slip motion and stability of a single degree of freedom elastic system with rate and state dependent friction, *J. Mech. Phys. Solids* **32,** 167–196.

Gu, Y. and T. Wong (1991). Effects of loading velocity, stiffness, and inertia on the dynamics of a single degree of freedom spring-slider system, *J. Geophys. Res.* **96,** 21677–21691.

Gutenberg, B. (1945). Amplitudes of surface waves and magnitudes of shallow earthquakes, *Bull. Seism. Soc. Am.* **35,** 3–12.

Hanks, T. C. and H. Kanamori (1979). A moment magnitude scale, *J. Geophys. Res.* **84,** 2348–2350.

Harris, R. and R. W. Simpson (1992). Changes in static stress on southern California faults after the 1992 Landers earthquake, *Nature* **360,** 251–254.

Harris, R., R. W. Simpson, and P. A. Reasenberg (1995). Influence of static stress changes on earthquake locations in southern California, *Nature* **385,** 221–224.

Heaton, T. H. (1982). Tidal triggering of earthquakes, *Bull. Seism. Soc. Am.* **72,** 2181–2200.

Hill, D. P., P. A. Reasenberg, A. Michael, W. J. Arabasz, G. Beroza, D. Brumbaugh, J. N. Brune, R. Castro, S. Davis, D. dePolo, W. L. Ellsworth, J. Gomberg, S. Harmsen, L. House, S. M. Jackson, M. John-

ston, L. Jones, R. Keller, S. Malone, L. Munguia, S. Nava, J. C. Pechmann, A. Sanford, R. W. Simpson, R. S. Smith, M. Stark, M. Stickney, A. Vidal, S. Walter, V. Wong, and J. Zollweg (1993). Seismicity remotely triggered by the magnitude 7.3 Landers, California, earthquake, *Science* **260,** 1617–1623.

Hill, D. P., M. J. S. Johnston, and J. O. Langbein (1995). Response of Long Valley caldera to the Mw = 7.3 Landers, California, earthquake, *J. Geophys. Res.* **100,** 12985–13005.

Jaume, S. C. and L. R. Sykes (1992). Changes in state of stress on the southern San Andreas fault resulting from the California earthquake sequence of April to June, 1992, *Science* **258,** 1325–1328.

Jaume, S. C. and L. R. Sykes (1996). Evolution of moderate seismicity in the San Francisco Bay region, 1850 to 1993: seismicity changes related to the occurrence of large and great earthquakes, *J. Geophys. Res.* **101,** 765–790.

Kagan, Y. Y. and D. D. Jackson (1991). Long-term earthquake clustering, *Geophys. J. Int.* **104,** 117–133.

Kanamori, H. (1972). Relation between tectonic stress, great earthquakes, and earthquake swarms, *Tectonophysics* **14,** 1–12.

Keilis-Borok, V. I. and V. G. Kossobokov (1990). Premonitory activation of earthquake flow: algorithm M8, *J. Earth Planet. Interiors* **61,** 73–83.

King, G. C. P., R. S. Stein, and J. Lin (1994). Static stress changes and the triggering of earthquakes, *Bull. Seism. Soc. Am.* **84,** 935–953.

Kossobokov, V. G. and J. M. Carlson (1995). Active zone size versus activity: a study of different seismicity patterns in the context of the prediction of algorithm M8, *J. Geophys. Res.* **100,** 6431–6441.

Linker, M. F. and J. H. Dieterich (1992). Effects of variable normal stress on rock friction: observations and constitutive equations, *J. Geophys. Res.* **97,** 4923–4940.

Marone, C., C. B. Raleigh, and C. H. Scholz (1990). Frictional behavior and constitutive modeling of simulated fault gouge, *J. Geophys. Res.* **95,** 7007–7025.

Marone, C. and B. Kilgore (1993). Scaling of the critical slip distance for seismic faulting with shear strain in fault zones, *Nature* **362,** 618–621.

Pepke, S. L., J. M. Carlson, and B. E. Shaw (1994). Prediction of large events on a dynamical model of a fault, *J. Geophys. Res.* **99,** 6769–6788.

Poley, C. M., A. G. Lindh, W. H. Bakun, and S. S. Schulz (1987). Temporal changes in microseismicity and creep near Parkfield, California, *Nature* **327,** 134–136.

Press, F. and C. Allen (1995). Patterns of seismic release in the southern California region, *J. Geophys. Res.* **100,** 6421–6430.

Press, W. H., B. P. Flannery, S. A. Teukolsky, and W. T. Vetterling (1986). Integration of ordinary differential equations, *Numerical Recipes, The Art of Scientific Computing,* Chap. 15, Cambridge Univ. Press, Cambridge, England, 550–559.

Protti, M., K. McNally, J. Pacheco, V. Gonzalez, C. Montero, J. Segura, J. Brenes, V. Barboza, E. Malavassi, F. Guendel, G. Simila, D. Rojas, A. Velasco, and A. Mata (1995). The March 25, 1990 (Mw = 7.0, ML = 6.8), earthquake at the entrance of the Nicoya Gulf, Costa Rica: its prior activity, foreshocks, and triggered seismicity, *J. Geophys. Res.* **100,** 20345–20358.

Reasenberg, P. A. and R. W. Simpson (1992). Response of regional seismicity to the static stress change produced by the Loma Prieta earthquake, *Science* **255,** 1687–1690.

Rice, J. and J. Gu (1983). Earthquake after effects and triggered seismic phenomena, *Pageoph* **121,** 187–219.

Rice, J. R. and A. L. Ruina (1983). Stability of steady frictional slipping, *J. Appl. Mech.* **105,** 343–349.

Rice, J. R. and S. T. Tse (1986). Dynamic motion of a single degree of freedom system following a rate and state dependent friction law, *J. Geophys. Res.* **91,** 521–530.

Roy, M. and C. Marone (1996). Earthquake nucleation on model faults with rate and state-dependent friction: the effects of inertia, *J. Geophys. Res.* **101,** 13919–13932.

Ruina, A. (1983). Slip instability and state variable friction laws, *J. Geophys. Res.* **88,** 10359–10370.

Rydelek, P. A., I. S. Sacks, and R. Scarpa (1992). On tidal triggering of earthquakes at Campi Flegrei, Italy, *Geophys. J. Int.* **109,** 125–137.

Savage, J. C., M. Lisowski, and W. H. Prescott (1990). An apparent shear zone trending north-northwest across the Mojave Desert into Owens Valley, eastern California, *Geophys. Res. Lett.* **17,** 2113–2116.

Scholz, C. H. (1990). *The Mechanics of Earthquakes and Faulting,* Cambridge U. Press, New York, 439 pp.

Segall, P. and J. R. Rice (1995). Dilatancy, compaction, and slip instability of a fluid-infiltrated fault, *J. Geophys. Res.* **100,** 22155–22173.

Simpson, R. W., S. S. Schulz, L. D. Dietz, and R. O. Burford (1988). The response of creeping parts of the San Andreas fault to earthquakes on nearby faults: two examples, *Pageoph* **126,** 665–685.

Singh, S. K., J. G. Anderson, and M. Rodriguez (1996). Triggered seismicity from major Mexican earthquakes, *Bull. Seism. Soc. Am.* (submitted).

Sleep, N. H. (1995). Ductile creep, compaction, and rate and state dependent friction within major fault zones, *J. Geophys. Res.* **100,** 13065–13080.

Sleep, N. H. and M. L. Blanpied (1992). Creep, compaction, and the weak rheology of major faults, *Nature* **359,** 687–692.

Sleep, N. H. and M. L. Blanpied (1994). Ductile creep and compaction: a mechanism for transiently increasing fluid pressure in mostly sealed fault zones, *Pageoph* **143,** 9–40.

Spudich, P., L. K. Steck, M. Hellweg, J. B. Fletcher, and L. M. Baker (1995). Transient stresses at Parkfield, California, produced by the M 7.4 Landers earthquake of June 28, 1992: observations from the UPSAR dense seismograph array, *J. Geophys. Res.* **100,** 675–690.

Stark, M. A. and S. D. Davis (1996). Remotely triggered microearthquakes at The Geysers geothermal field, California, *Geophys. Res. Lett.* **23,** 945–948.

Stein, R. S. and M. Lisowski (1983). The 1979 Homestead Valley earthquake sequence, California: control of aftershocks and postseismic deformation, *J. Geophys. Res.* **88,** 6477–6490.

Stein, R. S., G. C. P. King, and J. Lin (1992). Change in failure stress on the southern San Andreas fault system caused by the 1992 Magnitude = 7.4 Landers earthquake, *Science* **258,** 1328–1332.

Stuart, W. D. and T. E. Tullis (1995). Fault model for preseismic deformation at Parkfield, California, *J. Geophys. Res.* **100,** 24079–24101.

Tse, S. and J. Rice (1986). Crustal earthquake instabilities in relation to the depth variation of frictional slip properties, *J. Geophys. Res.* **91,** 9452–9572.

Tullis, T. E. and J. D. Weeks (1986). Constitutive behavior and stability of frictional sliding of granite, *Pure Appl. Geophys.* **124,** 384–414.

Wong, T., Y. Gu, T. Yanagidani, and Y. Zhao (1992). Stabilization of faulting by cumulative slip, in *Fault Mechanics and Transport Properties in Rocks,* B. Evans and T. Wong (Editors), Academic, London, 109–133.

USGS
CERI, University of Memphis
Campus Box 526590
Memphis, Tennessee 38112-6590
gomberg@usgs.gov
(J.G.)

USGS, MS 977
345 Middlefield Rd.
Menlo Park, California 94025
mblanpied@usgs.gov, nbeeler@usgs.gov
(M.B., N.B.)

Manuscript received 3 July 1996.